# Macromolecular Complex Including Mixed Lineage Leukemia 3, Carabin and Calcineurin Regulates Cardiac Remodeling

Roberto Pane, Loubna Laib, Karina Formoso, Maximin Détrait, Yannis Sainte-Marie, Florence Bourgailh, Nolan Ruffenach, Hanamée Faugeras, Ilias Simon, Emeline Lhuillier, et al.

**Title:** Macromolecular complex including Mixed Lineage 1 Leukemia 3, Carabin and calcineurin regulates cardiac remodelling

**Authors:**
Caroline Conte (Inserm UMR-1297)
Roberto Pane (Inserm UMR-1297)
Loubna Laib (Inserm UMR-1297)
Karina Formoso (Inserm U1297)
Maximin Détrait (Univ. Grenoble Alpes, Inserm, CHU Grenoble Alpes, HP2)
Yannis Sainte-Marie (Inserm/UPS UMR1297)
Florence bourgailh (Inserm UMR-1297)
Nolan Ruffenach (Inserm UMR-1297)
Hanamée Faugeras (Inserm UMR-1297)
Ilias Simon (Inserm UMR-1297)
Emeline Lhuillier (I2MC INSERM U1297)
Frank Lezoualc'h (Institute of Metabolic and Cardiovascular diseases, INSERM, University of Toulouse, UMR-1297)

# Macromolecular complex including Mixed Lineage Leukemia 3, Carabin and Calcineurin regulates cardiac remodelling

Roberto Pane[1*], Loubna Laib[1*], Karina Formoso[1], Maximin Détrait[1], Yannis Sainte-Marie[1], Florence Bourgailh[1], Nolan Ruffenach[1], Hanamée Faugeras[1], Ilias Simon[1], Emeline Lhuillier[1,2], Frank Lezoualc'h[1†¶], Caroline Conte[1†¶]

[1]Institut des Maladies Métaboliques et Cardiovasculaires, Inserm,
Université de Toulouse III-Paul Sabatier,
UMR 1297-I2MC,
31432 Toulouse, France
[2]GeT-Sante, Plateforme Genome et Transcriptome, GenoToul, Toulouse, France

[*]Co-first authorship
[†]Co-senior authorship

Short title: MLL3 promotes cardiac remodelling

[¶]Corresponding authors:

Frank Lezoualc'h
Institut des Maladies Métaboliques et Cardiovasculaires
Université de Toulouse III-Paul Sabatier
Inserm UMR 1297-I2MC
31432 Toulouse, France
Frank.Lezoualch@inserm.fr

Caroline Conte
Institut des Maladies Métaboliques et Cardiovasculaires
Université de Toulouse III-Paul Sabatier
Inserm UMR 1297-I2MC
31432 Toulouse, France
Caroline.Conte@inserm.fr

Total word count: 7017

## ABSTRACT

**BACKGROUND:** Cardiac hypertrophy is an intermediate stage in the development of heart failure (HF). The structural and functional processes occurring in cardiac hypertrophy include extensive gene reprogramming which is dependent on epigenetic regulation and chromatin remodelling. However, the chromatin remodelers and their regulatory functions involved in the pathogenesis of cardiac hypertrophy are not well characterized.

**METHODS:** Protein interaction was determined by immunoprecipitation assay in primary cardiomyocytes and mouse cardiac samples subjected or not to transverse aortic constriction (TAC) for one week. Chromatin Immunoprecipitation and DNA sequencing (ChIP-seq) experiments were performed on the chromatin of adult mouse cardiomyocytes.

**RESULTS:** We report that the calcium-activated protein phosphatase Calcineurin, its endogenous inhibitory protein Carabin, the STE20-like protein kinase 3 (STK24) and the histone monomethyltransferase, Mixed Lineage Leukemia 3 (MLL3) form altogether a macromolecular complex at the chromatin of cardiomyocytes. Under basal conditions, Carabin prevents Calcineurin activation while the serine/threonine kinase STK24 maintains MLL3 inactive via phosphorylation. After one week of TAC, both Carabin and STK24 are released from the Calcineurin-MLL3 complex leading to the activation of Calcineurin, dephosphorylation of MLL3 and in turn histone H3 lysine 4 monomethylation. Selective cardiac MLL3 knock-down mitigates hypertrophy and ChIP-seq analysis demonstrates that MLL3 is *de novo* recruited at the transcriptional start site of genes implicated in cardiomyopathy in stress conditions. We also show that Calcineurin and MLL3 co-localize at chromatin and that Calcineurin activates MLL3 histone methyl transferase activity at distal intergenic regions under hypertrophic conditions.

**CONCLUSIONS:** Our study reveals an unsuspected epigenetic mechanism of Calcineurin that directly regulates MLL3 histone methyl transferase activity to promote cardiac remodelling.


**Key Words:** Histone methyltransferase ; Calcineurin ; cardiac hypertrophy ; gene reprogramming

## INTRODUCTION

When subjected to pathological stress such as myocardial infarction, the heart undergoes a dynamic process of ventricular remodelling, which includes morphological modifications of the ventricular wall associated with increased cardiomyocyte size[1]. Although this myocardial hypertrophic growth response is adaptative in the short term, sustained stress over time can promote cardiac contractile dysfunction leading to the development of heart failure (HF), a major cause of death worldwide with no curative treatment[1–4]. Maladaptive cardiac hypertrophy is associated with a reprogramming of gene expression, which consists of the re-expression of foetal cardiac genes in adult cardiomyocytes and dysregulation of genes involved in metabolism, calcium handling and matrix remodelling[5]. These alterations of physiological gene expression play a causative role in pathological cardiac remodelling and the pathogenesis of HF[5–7].

Histone-modifying enzymes are important regulators of gene transcription regulation[8]. Although the role and molecular mechanisms of histone deacetylases (HDAC) have been well documented in pathological cardiac hypertrophy and HF[9–11], the involvement of other epigenetic enzymes and their interaction with canonical pro-hypertrophic signalling pathways in cardiac disease conditions remain poorly studied. High-throughput protein-associated DNA fragment sequencing (ChIP-seq) analysis in human failing heart samples and in experimental rodent models of HF has revealed a specific epigenetic signature defined by histone acetylation and methylation at transcriptional regulatory elements associated with cardiac hypertrophy [12,13] . In particular, the H3K4 and H3K9 methylation profiles at genomic regions containing genes implicated in intracellular calcium regulation or cardiac contractility have been shown to be altered in response to cardiac stress[13]. Some of the enzymes involved in histone methylation profiling in response to hypertrophic cardiac stress have been identified. For instance, the H3K9 dimethyltransferase EHMT1/2 has been reported to prevent cardiac

hypertrophy development through the repression of cardiac fetal genes[14]. However, further studies are required to understand how the activity and recruitment of these histone-modifying enzymes are regulated under cardiac stress.

One of the major pro-hypertrophic signalling factors in cardiomyocytes is the serine/threonine phosphatase Calcineurin, which activates its downstream effector nuclear factor of activated T cells (NFAT) to regulate gene expression[15,16]. Here, we identified the histone methyltransferase (HMT) Mixed Lineage Leukemia 3 (MLL3) (also named KMT2C) as a molecular partner of Calcineurin and its endogenous inhibitory protein Carabin. We found that a macromolecular complex formed of Calcineurin, Carabin, MLL3 and the STE20-like protein kinase 3 (STK24) regulates cardiac remodelling through modulation of histone H3 lysine 4 (H3K4) monomethylation at distal intergenic regions in response to cardiac stress.

# METHODS

## Data Availability

ChIP-seq raw data have been deposited to the ENA repository with accession number PRJEB50435. The other data that support the findings of this study are available in the Supplemental Data. Some key data, uncropped gels and detailed descriptions of materials and methods are available in the Supplemental Data.

Additional methods or data can be obtained from the corresponding authors upon reasonable request.

## Statistical analysis

The statistical analyses were performed with GraphPad Prism 9.5. Results were expressed as mean±SEM. P-values less than 0.05 were considered significant.

Non-parametric tests were employed to assess group differences in experiments with $N<10$ or showing dispersed data or heteroscedasticity. Mann-Whitney tests were used to compare 2 conditions and Kruskal-Wallis or Friedman tests were used to compare respectively, paired and unpaired data for more than 2 compared groups. These tests were corrected using False Discovery Rate for multiple comparisons.

For $N>10$ showing normality and homoscedasticity, ordinary one-way ANOVA tests corrected with Sidak's or Tukey's multiple comparisons tests were performed.

# RESULTS

## Carabin interacts with MLL3

We previously characterized Carabin, an endogenous inhibitor of Calcineurin that prevents maladaptive cardiac hypertrophy and progression to HF[17]. To better understand the molecular mechanisms underlying the cardioprotective effect of Carabin, we performed a yeast two-hybrid (Y2H) screen using a human heart cDNA library and full-length Carabin as bait. Almost half of Carabin putative binding partners (22 out of 47) were nuclear proteins (Figure 1A) and their clustering revealed that most of them (65%) corresponded to transcription factors (39%) and chromatin remodellers (26%) (Figure 1A, Supplemental Table 1). In line with its potential nuclear action, Carabin displayed a stronger nuclear localization in primary neonatal ventricular myocytes (NRVM) treated with the pro-hypertrophic stimulus, phenylephrine (PE) (10 μM, 24 h) compared with untreated cells (Figure S1A). In addition, Carabin interacted with histone H3 within chromatin, suggesting direct participation of Carabin in chromatin remodelling macromolecular complexes (Figure 1B). Accordingly, size-exclusion chromatography showed that Carabin was eluted and detected in a high molecular weight fraction (>1.5 MDa) in unstimulated NRVM (Figure 1C). Notably, Carabin was identified in lower weight (0.3-0.7 MDa) molecular complexes under hypertrophic condition (Figure 1C) indicating that Carabin dissociated from a macromolecular complex in response to a stress signal.

Immunoprecipitation experiments and immunoblot analysis demonstrated that the HMT MLL3 identified in the Y2H screen interacted with Carabin in mouse heart samples, isolated adult rat cardiomyocytes and NRVM (Figures 1D, S1B, S1C). Importantly, Carabin dissociated from the histone H3 and the interaction of Carabin with MLL3 complex decreased under hypertrophic conditions (PE treatment) in neonatal and adult rat cardiomyocytes (S1B, S1C, 1E). Similarly, the release of Carabin from MLL3 was also observed in mouse hearts

subjected to 1 week transaortic constriction (TAC) (Figure 1D), a time-point corresponding to the early phase of cardiac hypertrophy when the hypertrophic-specific epigenetic signature is present [12,18]. As expected, Carabin also dissociated from a well-known sub-unit of MLL3, WD-40 repeat protein-5 (WDR5)[19] after 1 week TAC (Figure 1D).

Since MLL3 displays an H3K4 monomethylase activity [20,21], we measured H3K4 monomethylation (H3K4Me1) level in hearts of control or failing patients. The expression of MLL3 and its partner WDR5 increased and correlated with the augmentation of H3K4Me1 level in human failing hearts (Figures 1F, 1G, S1D, S1E). Myocardial MLL3 protein level was also augmented 4 weeks after TAC, a stage corresponding to pathological cardiac remodelling in mouse [18] (Figures 1H). Interestingly, an increase of H3K4Me1 level in one week post-TAC mouse hearts was observed while MLL3 protein expression was unchanged at this early stage of cardiac remodelling (Figure 1I, S1F). In addition, *in vivo* knock-down of MLL3 using a cardiotropic adeno-associated virus serotype 9 (AAV9) expressing *mll3*-targeted shRNAs (AAV9-shMLL3) prevented 1 week TAC-induced H3K4Me1 increase (Figures 1I, S1G). These data indicate that MLL3 activity increases at the onset of cardiac hypertrophy and promotes a global augmentation of H3K4Me1 epigenetic mark.

Altogether, these findings suggest a role of Carabin in the development of the hypertrophic epigenome which induces the expression of a pathological gene program at the onset of cardiac stress.

**Carabin and Calcineurin exert an antagonist effect on MLL3-induced H3K4Me1 increase**

Next, we sought to determine the effect of Carabin on MLL3 HMT activity. Consistent with the results obtained in mouse hearts, both nuclear MLL3 expression and HMT activity were increased in hypertrophied cardiomyocytes (Figures 2A, S2A). Conversely, silencing MLL3

with a specific siRNA (siMLL3) prevented PE-induced H3K4Me1 in NRVM (Figures 2B, S2B). Interestingly, a siRNA against Carabin (siCarab) mimicked the stimulating effect of PE on H3K4Me1, as it induced a 2.5-fold increase in global H3K4Me1 in control condition (Figure 2B). In addition, siCarab-induced H3K4Me1 increase was prevented in siMLL3-transfected NRVM, indicating that Carabin specifically blocked MLL3 HMT activity in unstimulated cardiomyocytes (Figure 2B). Finally, we determined the mechanisms by which Carabin decreased MLL3 HMT activity. Because Carabin interacts with Calcineurin and inhibits its activity[17,22], we assessed whether Calcineurin could regulate MLL3 HMT activity. As expected, a potent pharmacological inhibitor of Calcineurin, cyclosporine (CsA), prevented PE-induced H3K4Me1 level in NRVM (Figure 2C). Carabin overexpression reproduced the effect of CsA on H3K4Me1 while CsA and Carabin had no synergistic action (Figure 2C). In addition, knock-down of Calcineurin with a siRNA (siCaN) prevented MLL3-dependent increase of H3K4Me1 induced by PE (Figures S2C, S2D). These results indicate that Carabin and Calcineurin display antagonist effects on MLL3 HMT activity in cardiomyocytes. Finally, we demonstrated that siMLL3 decreased various cardiomyocyte hypertrophic markers including cardiomyocyte size, *nppb* and *acta1* expression in NRVM treated with either PE or the prohypertrophic peptide, Angiotensin II (Ang II) (Figures 2 D-F, S2E).

**MLL3 promotes cardiac hypertrophy**

Next, we investigated the impact of MLL3 knock-down in the development of cardiac hypertrophy using an AAV9-based gene transfer approach (Figures S1G-H, S2F). Echocardiography analysis showed that cardiac function in one-week TAC mice was comparable with Sham operated mice treated with either an AAV9 encoding an untargeted shRNA control (AAV9-shCT) or AAV9-shMLL3 (Table 1). However, the increase in left

ventricular anterior wall thickness (LVAW) observed in the TAC group was significantly reduced in AAV9-shMLL3 injected-mice (Table 1). Consistently, MLL3 knock-down decreased cardiomyocyte cross-sectional area and the expression of the cardiac foetal genes, *nppb*, *acta1* and *myh-7* after TAC (Figures 3A, B). Importantly, cardiac MLL3 knock-down reduced cardiac hypertrophy and lung oedema in 6 weeks post-TAC mouse hearts compared to TAC mice treated with AAV9-shCT (Figures 3C-D, S1H, Table 2). Consistently, cardiac function was ameliorated in post-TAC mouse hearts treated with AAV9-shMLL3 (Figure 3E). These results indicate that decreased MLL3 expression prevents TAC-induced cardiac hypertrophy and HF development.

To further understand the mechanism of MLL3 induced cardiac hypertrophy, MLL3-targeted Chromatin Immunoprecipitation and DNA sequencing (ChIP-seq) experiments were performed on chromatin of cardiomyocytes isolated from one-week Sham or TAC mouse hearts (Figure 4A). We found an increase of MLL3 recruitment on chromatin of cardiomyocytes isolated from TAC mice (Figure 4B). Indeed, 205 and 375 genomic regions were targeted by MLL3 in Sham and TAC conditions, respectively while 122 genomic regions were targeted in both conditions showing a redistribution of MLL3 recruitment in response to cardiac stress (Figures 4B, S3A-B, Supplemental Table 2) (p-value from the hypergeometric test for Sham and TAC overlapping = 0). Notably, while the chromatin recruitment of MLL3 was mainly observed in distal intergenic regions under basal condition, it was predominantly increased in the transcriptional start site (TSS) regions (<1 kb) (p-value in TAC condition = 7.5e-45, p-value in sham condition = 0.1039578 using hypergeometric tests) and represented 38.4% of the targeted regions at the onset of hypertrophy (Figures 4C, S3C-E). In addition, the overlaps of MLL3 genomic loci with ATAC- and histone marks ChIP-seq published data[23] showed that 193 out of the 375 (51.47%) TAC-specific MLL3

bound genomic regions corresponding mainly to promoter targeted regions (123 out of 193) were located in opened chromatin (Figures 4D, Supplemental Table 2). Interestingly, 21 of the 124 genes targeted by MLL3 on their promoter regions were dysregulated in TAC condition (Figure 4E). Among them, 14 genes were upregulated suggesting that MLL3 recruitment at promoters is correlated with an increased transcriptional activation of its target genes (p=0.027) (Figure 4E). Under basal conditions, only 27 out of the 205 (13.17%) specific MLL3 bound genomic regions were found localized in opened chromatin. Interestingly, some TAC-specific MLL3 bound intergenic regions or located in gene bodies showed an increase of DNA accessibility in response to cardiac stress (Figures 4D, Supplemental Table 2), thus suggesting a potential role of MLL3 in chromatin opening.

Gene set enrichment analysis of MLL3 ChIP-seq data obtained in TAC condition showed an enrichment of MLL3 recruitment in proximity of or at various genes implicated in cardiomyopathy and cardiac sarcomerogenesis including *atp2a2*, *atp5j, HDAC7 Myh6*, *Ttn*, and *Tnnt2* (Figures 4F, S3F). ChIP-qPCR experiments further confirmed an increased MLL3 binding at the TSS of *atp5j* and *tnnt2* (Figures 4G-H).

Altogether, these data suggest that MLL3 promotes cardiac hypertrophy through its *de novo* recruitment at the TSS leading to transcriptional activation of genes involved in cardiomyopathy.

**The Ser/Thr kinase STK24 counteracts Calcineurin-dependent activation of MLL3**

Interestingly, MLL3 interacted with Carabin mainly under basal condition whereas it associated with Calcineurin, but not its downstream classical target, NFAT under normal and hypertrophic conditions in NRVM as well as in adult rat cardiomyocytes and mouse hearts (Figures 5A, S1B-C, S4A, S4C). This suggests that, in basal state, Carabin interacts with the Calcineurin-MLL3 complex and maintains MLL3 inactive via its inhibitory action on

Calcineurin in cardiomyocytes. On the contrary, under hypertrophic condition Carabin was released from the Calcineurin-MLL3 complex (Figures 5A, S4A, S4C), and relieved its tonic inhibition on the phosphatase Calcineurin, thus enhancing MLL3 activity (Figures 2B-C, S2D).

In line with this, hypertrophic stress decreased MLL3 serine-specific phosphorylation (Figures 5B, S4B), which was prevented by CsA treatment (Figure 5C). Of particular importance, the Carabin Y2H screen revealed a STE20-like protein kinase 3 kinase named MST3 or STK24 (Supplemental Table 1), which is highly enriched in both rat cardiomyocytes and human hearts[24]. In response to PE treatment, STK24 protein level remained unchanged (Figure S5A). However, a strong decrease in STK24 autophosphorylation level which is indicative of STK24 activity [25] was observed in PE-stimulated NRVM, (Figure S5A).

Immunoprecipitation experiments showed that indeed STK24 interacted with Carabin and MLL3 in NRVM, adult rat cardiomyocytes and mouse hearts (Figures 5A, S4A, S4C). Strikingly, the interaction of STK24 with MLL3 observed in basal condition was highly reduced in PE-stimulated cardiomyocytes and in TAC hearts (Figures 5A, S4A, S4C, S4E) while the autophosphorylation level of the MLL3-interacting STK24 remained unchanged (Figures S4C, S4F). Silencing STK24 expression with a specific siRNA (siSTK24) diminished MLL3 phosphorylation and activated foetal gene expression in unstimulated NRVM without affecting Calcineurin or Carabin protein levels (Figures 5D, S5C, S5D). Importantly, the effect of siSTK24 on MLL3 phosphorylation translated on its HMT activity since siSTK24 transfected cells displayed a 2.5-fold increase in MLL3-induced H3K4Me1 under basal condition, while STK24 knock-down did not influence H3K4Me1 levels in PE-treated NRVM (Figure 5E). Finally, consistent with an anti-hypertrophic action of STK24,

Calyculin, a potent STK24 pharmacological activator[26] reduced the expression of hypertrophic markers and H3K4Me1 in PE treated NRVM (Figure S5E, S5F) .

Altogether, these results show that, under basal condition, STK24, Calcineurin, Carabin and MLL3 form a macromolecular complex in which Carabin blocks Calcineurin activation and STK24 maintains MLL3 inactive via phosphorylation. In response to hypertrophic stress, Carabin and STK24 are released from MLL3-Calcineurin complex leading to Calcineurin phosphatase activation, which dephosphorylates MLL3 to promote MLL3 HMT activation (Figure 5F).

**Calcineurin activates MLL3 HMT activity at distal intergenic regions**

ChIP-seq experiments demonstrated that Calcineurin bound to chromatin in cardiomyocytes isolated from one-week Sham or TAC hearts (Figure 6A). Specifically, Calcineurin was more abundant in chromatin in basal condition than in TAC group (448 genomic regions in Sham versus 169 in TAC) and its localization was redistributed in response to cardiac stress (Figures 6A, S6A-C) (p-value from the hypergeometric test for Sham and TAC overlapping = 0). Under basal condition, Calcineurin was mainly located at distal intergenic regions in proximity of genes implicated in calcium transport (Figures 6B-C). Importantly, *de novo* MEME motif discovery analysis of enriched DNA sequences within the Calcineurin binding regions in Sham or TAC conditions revealed specific DNA motifs showing similarities with binding sites of some transcription factors known to be involved in Calcineurin signalling (Figure 6D). Among them, we identified ETS2 (a member of the E26 transformation-specific sequence [ETS] domain family), Interferon regulatory factor 8 (IRF8) or NFatc4, which were previously reported to functionally interact with Calcineurin signalling during cardiac development and remodelling[27–29] (Figure 6D).

Heatmap visualization of the MLL3 binding at the Calcineurin binding sites showed a

stronger degree of MLL3 and Calcineurin co-bound regions in TAC (48%) than in Sham (31%) condition indicating that the interaction Calcineurin-MLL3 at their common loci was increased in cardiac hypertrophy (Figures 7A-B, S6D-F).

Of particular interest, we revealed a significant colocalization of MLL3 and Calcineurin (70 regions, p-value = 8.03e-303 in the hypergeometric test) on genomic regions targeted under both conditions (Figure 7C). These regions were mainly located in distal intergenic regions located near genes implicated in catabolic processes (*ddo*, *got2*), membrane repolarisation (*kcnj5*) or cardiac cell differentiation as well as atrial fibrillation (*nkx2-6*) (Figures 7D, S6G). To illustrate the impact of Calcineurin on MLL3 activity in response to hypertrophic stress, we measured H3K4Me1 level on two co-targeted sites at intergenic regions 6 and 17 (Figures 7E-F). As expected, the recruitment of the Calcineurin-MLL3 complex was associated with an increase of H3K4Me1 level under hypertrophic conditions when compared to control (Figures 7E-F). Altogether, these results showed that Calcineurin recruitment on chromatin is largely redistributed in response to cardiac hypertrophic stress indicating that Calcineurin is directly implicated in gene regulation under basal and cardiac stress condition. In addition, MLL3 and Calcineurin co-binding sites showed an increase of H3K4Me1 level under hypertrophic condition (Figures 7E-F). These data together with the stimulating effect of Calcineurin on MLL3 HMT activity indicate that this phosphatase can directly regulate chromatin remodelling through epigenetic enzyme activation.

## DISCUSSION

Our study identified a novel molecular complex including MLL3, Calcineurin and Carabin, which regulates cardiac hypertrophy development leading to HF. The kinase STK24 phosphorylates MLL3 causing its inactivation while the inhibitory effect of Carabin on Calcineurin prevents MLL3 dephosphorylation in basal condition. Under cardiac stress the release of Carabin and STK24 from the Calcineurin-MLL3 complex relieves inhibition of Calcineurin phosphatase activity. Subsequent MLL3 dephosphorylation switches on MLL3 HMT activity that leads to an increase in H3K4Me1 levels and consequently the expression of cardiac hypertrophy regulatory genes.

Previous studies demonstrated that MLL3 is involved in oncogenesis[30]. Here, we disclose a novel role for MLL3 in cardiac remodelling. Consistent with our finding on MLL3 pro-hypertrophic action, Jiang and Colleagues (2017) reported that MLL3 expression, but not that of other MLL members such as MLL2 and MLL4, was specifically increased in human dilated cardiomyopathy hearts and mouse cardiac samples subjected to TAC[31]. In addition, we found that MLL3 knock-down improves cardiac function in a mouse model of myocardial pressure overload. The effect of MLL3 correlates with its HMT activity and this translates on an overall increase in H3K4Me1 mark, which is most often associated with enhancer activation.

MLL3 is known as one of the major H3K4Me1 methyltransferases responsible for H3K4Me1 deposition at enhancers, which are essential in regulating cell-type-specific gene expression[32,33]. We found that MLL3 bound to DNA inaccessible intergenic regions under basal conditions. Interestingly, differential chromatin accessibility landscape revealed a TAC-induced increase of chromatin accessibility at some MLL3 bound-regions located in gene bodies or intergenic regions. These results suggest that MLL3 could cooperatively open chromatin at enhancers in response to cardiac stress. This is consistent with the identification

of an ATP-dependent chromatin remodeler, CHD8, in the Carabin Y2H and previous published data showing the presence of CHD8 in MLL complexes[34]. In contrast to physiological conditions, MLL3 was largely localised at the promoters (32%) in opened chromatin associated with typical opened chromatin histone marks (H3K4Me3, H3KAc) after TAC-induced myocardial pressure overload. The MLL3-dependent H3K4Me1 deposition on promoters is known to silence genes[35]. However, MLL3 can also enhance RNA pol II recruitment independent of its HMT activity[36]. Consistent with this, 21 of the MLL3 promoter-targeted genes were dysregulated and among them 14 were upregulated after TAC. These data suggest that MLL3 could act as a transcriptional activator when recruited on TSS in response to cardiac stress.

Calcineurin and its endogenous inhibitor, Carabin are key proteins involved in the development of cardiac hypertrophy leading to HF[17,37]. Their mechanisms of action have been mainly described in the cytosolic compartment where they regulate the phosphorylation state of the transcription factor NFAT and its subsequent nuclear translocation. However, Calcineurin has also been found in the nucleus and its nuclear import regulates cardiac hypertrophy development [38,39]. Our data demonstrate that Carabin is also present in a nuclear macromolecular chromatin complex in cardiomyocytes and interacts with the histone H3, a canonical component of nucleosomes. In line with this finding, Carabin was reported to associate with histone H4 in human promyelocytic leukaemia NB4 cells[40]. Importantly, the release of Carabin from the nuclear MLL3-Calcineurin complex leads to Calcineurin-dependent MLL3 activation and thus increases the H3K4Me1 mark at the onset of cardiac hypertrophy, which then leads to cardiac dysfunction. Besides its Calcineurin-interacting site that prevents Calcineurin activation, Carabin contains a functional Ras-GTPase activating protein (Ras-GAP) domain which inactivates Ras activity and, in turn, impairs downstream MAPK and ERK pro-hypertrophic signalling[17,22]. Whether the Ras-GAP domain of Carabin

influences histone post-translational modifications and chromatin activation has yet to be investigated.

Calcineurin ChIP-seq analyses revealed that the calcium-sensitive phosphatase was mainly enriched at intergenic regions, suggesting its involvement in gene enhancer regulation. Interestingly, GO analysis of genes located near Calcineurin bound sites showed molecular processes associated with calcium signalling. NFATC4 binding motif was significantly present in Calcineurin targeted regions in TAC hearts, suggesting that NFAT could be implicated in Calcineurin recruitment on chromatin. In addition, ChIP-seq analyses revealed that Calcineurin and MLL3 co-localized at 70 common regions in basal and stress conditions, which were mainly intergenic. However, Calcineurin but not NFAT interacted with MLL3 at chromatin and regulated MLL3 HMT activity under hypertrophic stimulus strengthening our assumption that MLL3 and Calcineurin cooperatively act in a novel NFAT-independent signalling pathway to regulate enhancer activity[33]. Of note, this novel function for Calcineurin in chromatin remodelling in cardiomyocytes is in line with the recent observation that this phosphatase promotes activation of Brg1, an enzymatic subunit of the mammalian SWI/SNF ATP-dependent chromatin remodelling enzyme in C2C12 myoblast line[41]. Since Calcineurin has been implicated in several other extra-cardiac biological function, its effect on chromatin remodelling might have more general implications in other cellular systems and diseases.

Epigenetics plays a central role in pathological cardiac remodeling leading to HF. Many studies are nowadays focusing on potential modulators of these pathways to slowdown or prevent the development of several cardiovascular disease[42]. In our study we identified a novel epigenetic mechanism through MLL3 that contributes to HF progression. Thus, this molecular complex could be an interesting target to develop novel therapeutic approaches.

## REFERENCES

1. Hill, J. A. & Olson, E. N. Cardiac plasticity. *N Engl J Med* **358**, 1370–1380 (2008).
2. Levy, D. *et al.* Risk of ventricular arrhythmias in left ventricular hypertrophy: the Framingham Heart Study. *Am J Cardiol* **60**, 560–565 (1987).
3. Schiattarella, G. G. & Hill, J. A. Inhibition of hypertrophy is a good therapeutic strategy in ventricular pressure overload. *Circulation* **131**, 1435–1447 (2015).
4. de Simone, G., Gottdiener, J. S., Chinali, M. & Maurer, M. S. Left ventricular mass predicts heart failure not related to previous myocardial infarction: the Cardiovascular Health Study. *Eur Heart J* **29**, 741–747 (2008).
5. Kehat, I. & Molkentin, J. D. Molecular pathways underlying cardiac remodeling during pathophysiological stimulation. *Circulation* **122**, 2727–2735 (2010).
6. Lompre, A. M. *et al.* Myosin isoenzyme redistribution in chronic heart overload. *Nature* **282**, 105–107 (1979).
7. Nakamura, M. & Sadoshima, J. Mechanisms of physiological and pathological cardiac hypertrophy. *Nat Rev Cardiol* **15**, 387–407 (2018).
8. Allis, C. D. & Jenuwein, T. The molecular hallmarks of epigenetic control. *Nat Rev Genet* **17**, 487–500 (2016).
9. Zhang, C. L. *et al.* Class II histone deacetylases act as signal-responsive repressors of cardiac hypertrophy. *Cell* **110**, 479–488 (2002).
10. Bagchi, R. A. & Weeks, K. L. Histone deacetylases in cardiovascular and metabolic diseases. *J Mol Cell Cardiol* **130**, 151–159 (2019).
11. Papait, R., Serio, S. & Condorelli, G. Role of the Epigenome in Heart Failure. *Physiol Rev* **100**, 1753–1777 (2020).
12. Papait, R. *et al.* Genome-wide analysis of histone marks identifying an epigenetic signature of promoters and enhancers underlying cardiac hypertrophy. *Proceedings of the National Academy of Sciences* **110**, 20164–20169 (2013).

13. Kaneda, R. *et al.* Genome-wide histone methylation profile for heart failure. *Genes Cells* **14**, 69–77 (2009).
14. Thienpont, B. *et al.* The H3K9 dimethyltransferases EHMT1/2 protect against pathological cardiac hypertrophy. *J Clin Invest* **127**, 335–348 (2017).
15. Molkentin, J. D. *et al.* A calcineurin-dependent transcriptional pathway for cardiac hypertrophy. *Cell* **93**, 215–228 (1998).
16. Chaklader, M. & Rothermel, B. A. Calcineurin in the heart: New horizons for an old friend. *Cell Signal* **87**, 110134 (2021).
17. Bisserier, M. *et al.* Carabin protects against cardiac hypertrophy by blocking calcineurin, Ras, and Ca2+/calmodulin-dependent protein kinase II signaling. *Circulation* **131**, 390–400; discussion 400 (2015).
18. Souders, C. A., Borg, T. K., Banerjee, I. & Baudino, T. A. Pressure Overload Induces Early Morphological Changes in the Heart. *The American Journal of Pathology* **181**, 1226–1235 (2012).
19. Shinsky, S. A. & Cosgrove, M. S. Unique Role of the WD-40 Repeat Protein 5 (WDR5) Subunit within the Mixed Lineage Leukemia 3 (MLL3) Histone Methyltransferase Complex. *J Biol Chem* **290**, 25819–25833 (2015).
20. Hu, D. *et al.* The MLL3/MLL4 branches of the COMPASS family function as major histone H3K4 monomethylases at enhancers. *Mol Cell Biol* **33**, 4745–4754 (2013).
21. Sze, C. C. & Shilatifard, A. MLL3/MLL4/COMPASS Family on Epigenetic Regulation of Enhancer Function and Cancer. *Cold Spring Harb Perspect Med* **6**, a026427 (2016).
22. Pan, F. *et al.* Feedback inhibition of calcineurin and Ras by a dual inhibitory protein Carabin. *Nature* **445**, 433–436 (2007).
23. Chapski, D. J. *et al.* Early adaptive chromatin remodeling events precede pathologic phenotypes and are reinforced in the failing heart. *J Mol Cell Cardiol* **160**, 73–86 (2021).

24. Fuller, S. J. *et al.* Cardiac protein kinases: the cardiomyocyte kinome and differential kinase expression in human failing hearts. *Cardiovasc Res* **108**, 87–98 (2015).
25. Lu, T.-J. *et al.* Inhibition of cell migration by autophosphorylated mammalian sterile 20-like kinase 3 (MST3) involves paxillin and protein-tyrosine phosphatase-PEST. *J Biol Chem* **281**, 38405–38417 (2006).
26. Fuller, S. J. *et al.* A novel non-canonical mechanism of regulation of MST3 (mammalian Sterile20-related kinase 3). *Biochem J* **442**, 595–610 (2012).
27. Luo, Y. *et al.* Cooperative Binding of ETS2 and NFAT Links Erk1/2 and Calcineurin Signaling in the Pathogenesis of Cardiac Hypertrophy. *Circulation* **144**, 34–51 (2021).
28. Jiang, D.-S. *et al.* IRF8 suppresses pathological cardiac remodelling by inhibiting calcineurin signalling. *Nat Commun* **5**, 3303 (2014).
29. Bushdid, P. B., Osinska, H., Waclaw, R. R., Molkentin, J. D. & Yutzey, K. E. NFATc3 and NFATc4 are required for cardiac development and mitochondrial function. *Circ Res* **92**, 1305–1313 (2003).
30. Wang, L. & Shilatifard, A. UTX Mutations in Human Cancer. *Cancer Cell* **35**, 168–176 (2019).
31. Jiang, D.-S. *et al.* The Histone Methyltransferase Mixed Lineage Leukemia (MLL) 3 May Play a Potential Role on Clinical Dilated Cardiomyopathy. *Mol Med* **23**, 196–203 (2017).
32. Froimchuk, E., Jang, Y. & Ge, K. Histone H3 lysine 4 methyltransferase KMT2D. *Gene* **627**, 337–342 (2017).
33. Lai, B. *et al.* MLL3/MLL4 are required for CBP/p300 binding on enhancers and super-enhancer formation in brown adipogenesis. *Nucleic Acids Res* **45**, 6388–6403 (2017).
34. Zhao, C. *et al.* Dual Requirement of CHD8 for Chromatin Landscape Establishment and Histone Methyltransferase Recruitment to Promote CNS Myelination and Repair. *Developmental Cell* **45**, 753-768.e8 (2018).

35. Cheng, J. *et al.* A role for H3K4 monomethylation in gene repression and partitioning of chromatin readers. *Mol Cell* **53**, 979–992 (2014).
36. Dorighi, K. M. *et al.* Mll3 and Mll4 Facilitate Enhancer RNA Synthesis and Transcription from Promoters Independently of H3K4 Monomethylation. *Mol Cell* **66**, 568-576.e4 (2017).
37. Molkentin, J. D. Calcineurin and beyond: cardiac hypertrophic signaling. *Circ Res* **87**, 731–738 (2000).
38. Kar, P. & Parekh, A. B. Distinct spatial Ca2+ signatures selectively activate different NFAT transcription factor isoforms. *Mol Cell* **58**, 232–243 (2015).
39. Hallhuber, M. *et al.* Inhibition of nuclear import of calcineurin prevents myocardial hypertrophy. *Circ Res* **99**, 626–635 (2006).
40. Valiuliene, G. *et al.* Belinostat, a potent HDACi, exerts antileukaemic effect in human acute promyelocytic leukaemia cells via chromatin remodelling. *J Cell Mol Med* **19**, 1742–1755 (2015).
41. Witwicka, H. *et al.* Calcineurin Broadly Regulates the Initiation of Skeletal Muscle-Specific Gene Expression by Binding Target Promoters and Facilitating the Interaction of the SWI/SNF Chromatin Remodeling Enzyme. *Mol Cell Biol* **39**, e00063-19 (2019).
42. Shi, Y. *et al.* Epigenetic regulation in cardiovascular disease: mechanisms and advances in clinical trials. *Signal Transduct Target Ther* **7**, 200 (2022).

## Data availability

ChIP-seq raw data have been deposited to ENA repository with accession number PRJEB50435.

## Acknowledgements

We acknowledge the members of our laboratory for helpful suggestions and insights. We acknowledge Hippolyte Audureau and Jesica Formoso for their contribution in cardiomyocyte cell surface quantification and statistical analysis respectively. We are grateful to Dr. Michel Puceat and Prof. Mauro Giacca for the critical reading of the manuscript. We acknowledge members of the UMS-006 facilities for animal housing (ENI) (UMS 006/INSERM/UPS, Anexplo/Genotoul Plateform). We acknowledge the support from We-Met I2MC (Alexandre Lucas) and from GeT-Santé technical (Frederic Martins) platforms. We acknowledge the IFB-Institut Francais de Bioinformatique core facility and the EBAI Bioinformatics school. We thank Profs. Olivier Lairez and Bertrand Marcheix for providing human cardiac samples.

F.L. was supported by grants from Institut National de la Santé et de la Recherche Médicale, Université de Toulouse III-Paul Sabatier, the French National Agency for Research (ANR-17-CE14, Fondation pour la Recherche Médicale (Programme “Equipes FRM 2016”, DEQ20160334892 ; “Equipes FRM 2021, EQU202103012601”), Fondation de France (00066331/00096289), Fédération Française de Cardiologie, GDR 3545 (RCPG-Physio-Med) and Hybrigenics. R.P. was recipient of a PhD training grant from Université de Toulouse III – Paul Sabatier and Groupe de Réflexion sur la Recherche Cardiovasculaire (G.R.R.C).

## Author Contributions

R.P., L.L., K.F., M.D. performed the experiments, analyzed data and wrote the methods manuscript; Y.S performed surgical experiments and cardiac function analysis, H.F. and I.S. performed the experiments, F.T. performed histological analysis, N.R. contributed to ChIP-Seq analysis, E.L. contributed to ChIP-Seq experiments, F.L. and C.C. designed and initiated the project, supervised the project and wrote the manuscript.

## Ethics declarations

The study protocol on human samples was approved by Toulouse University Hospital local ethic committee. Experiments performed on mice were approved by local regulatory committee CEEA-122 in accordance with the French Ministry for Research.

## Conflict of interest

None declared

**Correspondence and requests** for materials should be addressed to Caroline Conte (Caroline.Conte@inserm.fr) or Frank Lezoualc'h (Frank.Lezoualch@inserm.fr)

## Supplementary Information is available for this paper

**Supplemental Figures S1-S6**

**Uncropped blots**

**Supplemental Table 1:** Candidate proteins identified in the Carabin-targeted yeast-two-hybrid screen and their molecular and biological functions.

**Supplemental Table 2:** ChIP-seq and ATAC-seq data

**Supplemental Table 3**: Statistic analysis

**Detailed Methods**

**Supplemental material**

**Major Ressource Table**

**ARRIVE Checklist**

Figure 1

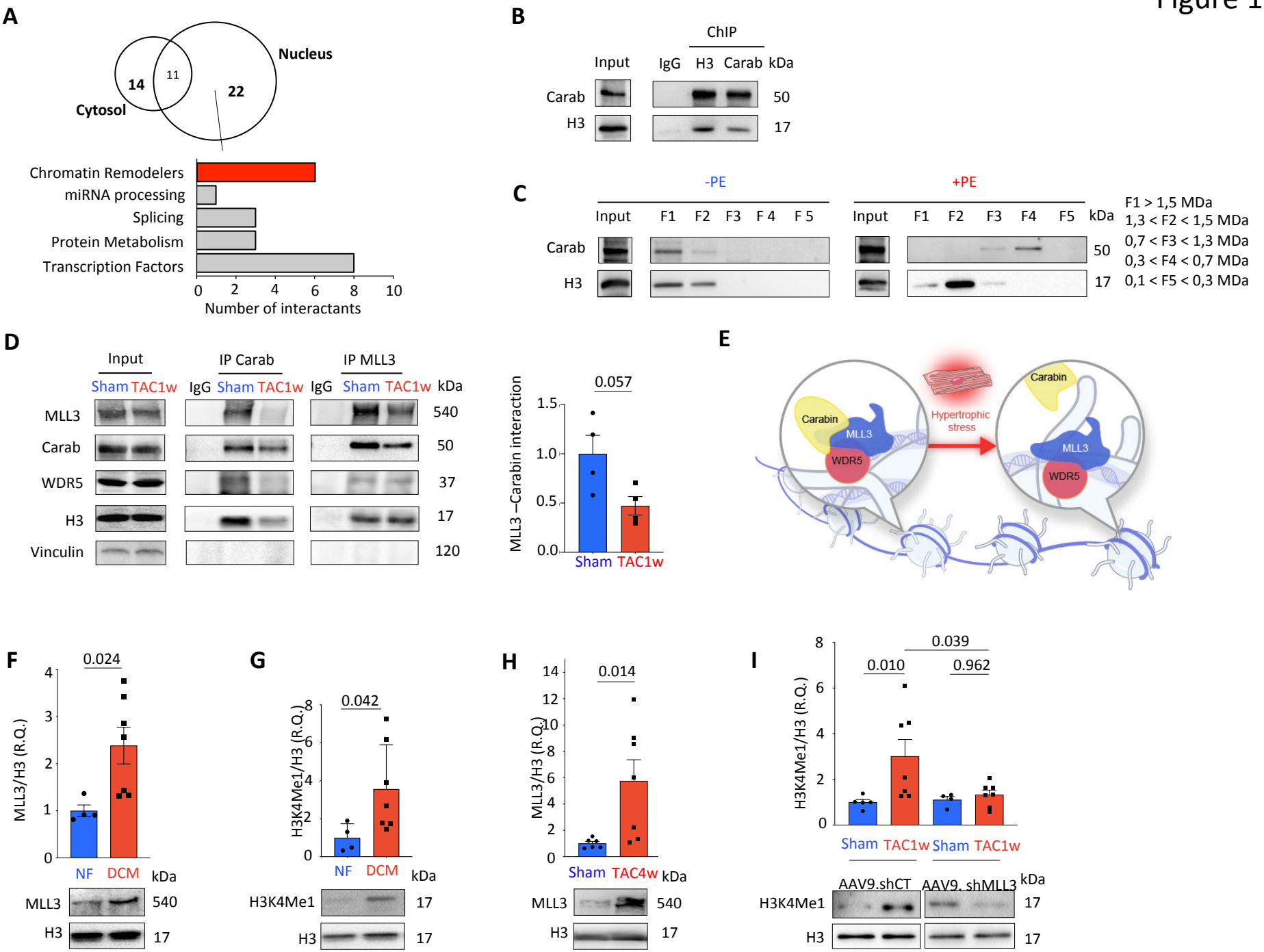
A
Nucleus
14
11
22
Cytosol
Chromatin Remodelers
miRNA processing
Splicing
Protein Metabolism
Transcription Factors
0 2 4 6 8 10
Number of interactants
B
ChIP
Input
IgG H3 Carab kDa
Carab
H3
50
17
C
-PE
+PE
Input F1 F2 F3 F 4 F 5
Input F1 F2 F3 F4 F5 kDa
Carab
H3
50
17
F1 > 1,5 MDa
1,3 < F2 < 1,5 MDa
0,7 < F3 < 1,3 MDa
0,3 < F4 < 0,7 MDa
0,1 < F5 < 0,3 MDa
D
Input
IP Carab
IP MLL3
Sham TAC1w IgG Sham TAC1w IgG Sham TAC1w kDa
MLL3
Carab
WDR5
H3
Vinculin
540
50
37
17
120
MLL3 –Carabin interaction
0.057
1.5
1.0
0.5
0.0
Sham TAC1w
E
Carabin
MLL3
WDR5
Hypertrophic stress
Carabin
MLL3
WDR5
F
0.024
MLL3/H3 (R.Q.)
4
3
2
1
0
NF DCM kDa
MLL3
H3
540
17
G
0.042
H3K4Me1/H3 (R.Q.)
8
6
4
2
0
NF DCM kDa
H3K4Me1
H3
17
17
H
0.014
MLL3/H3 (R.Q.)
14
12
10
8
6
4
2
0
Sham TAC4w kDa
MLL3
H3
540
17
I
0.039
0.010
0.962
H3K4Me1/H3 (R.Q.)
8
6
4
2
0
Sham TAC1w Sham TAC1w
AAV9.shCT AAV9. shMLL3 kDa
H3K4Me1
H3
17
17

**Figure 1. Carabin interacts with the histone methyl transferase MLL3.**

**A**, Cluster Maps of Carabin molecular partners identified by Y2H. **B**, ChIP followed by immunoblot showing Carabin (Carab) interaction with histone H3 in NRVM (n=3). **C,** Immunoblot analysis of Carabin in five fractions (F1-F5) obtained after size exclusion chromatography of protein extract from NRVM treated or not with PE (10 µM, 24 h) (n=3). Size of the protein complexes in the five fractions is shown on the right. **D,** Representative immunoblot after immunoprecipitation (IP) showing the interaction of Carabin with MLL3, WDR5 and histone H3 in mouse cardiac samples subjected or not (Sham) to one week TAC (TAC1w). Input is total lysates of tissue. Vinculin is a marker of the cytosolic compartment, H3 is a marker of chromatin. Histogram shows the ratio of immunoprecipitated Carabin to immunoprecipitated MLL3 in 4 independant experiments. **E**, Schematic representation of the impact of hypertrophic stress on the Carabin-MLL3-WDR5 complex in cardiomyocytes. **F-G**, Quantification of MLL3 protein expression (F) and H3K4Me1 levels (G) in left ventricular myocardium from patients with dilated cardiomyopathy (DCM, n=7) or non-failing (NF, n=4) control. **H,** Quantification of MLL3 protein expression in cardiac samples from mice subjected or not to 4-weeks TAC (n=6 in Sham and n=7 in TAC). **I**, Immunoblot analysis of H3K4Me1 levels in cardiac samples from mice injected with either AAV9-shCT or AAV9-shMLL3 and subjected or not to 1 week TAC (n=7 in both TAC groups ; n= 5 and 4 in sham mice injected with AAV9.shCT and AAV9.shMLL3 respectively).

Results are expressed as mean ± SEM relative to non-failing heart (Sham or NF) (D-H) and expressing ShCT (I). Differences between groups were analyzed by a Mann-Whitney U test (D, F, G, H). For (I), statistics analyses were performed on log-transformed values. Differences between groups were analyzed by a one-way ANOVA with Sidak's multiple comparisons test. Black lines indicate compared groups with the corresponding p-value. Differences were considered significant when $P<0.05$.

Figure 2

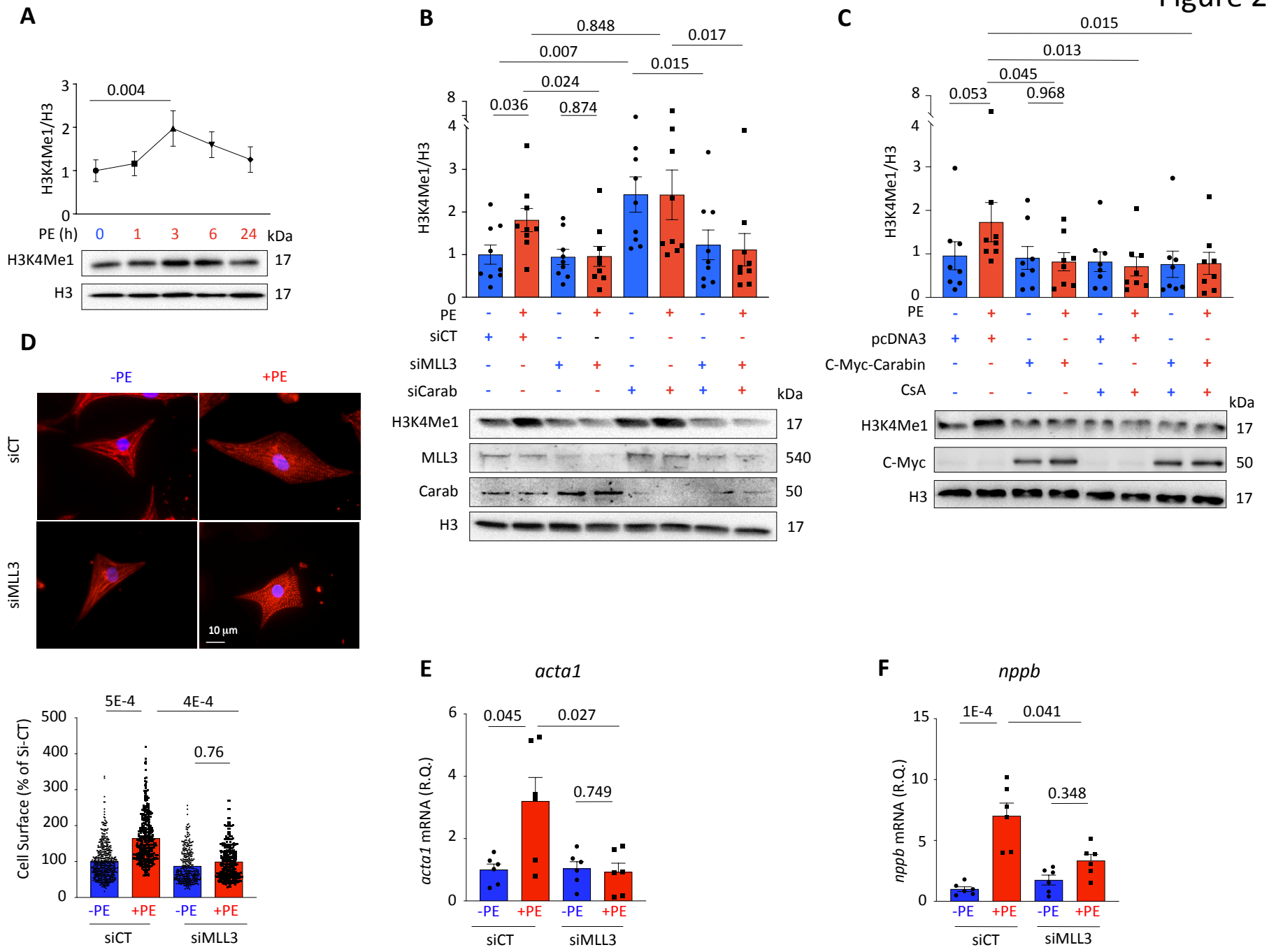
A
0.004
H3K4Me1/H3
PE (h) 0 1 3 6 24 kDa
H3K4Me1 17
H3 17
B
0.848
0.017
0.007
0.015
0.024
0.036
0.874
H3K4Me1/H3
PE
siCT
siMLL3
siCarab
kDa
H3K4Me1 17
MLL3 540
Carab 50
H3 17
C
0.015
0.013
0.045
0.053
0.968
H3K4Me1/H3
PE
pcDNA3
C-Myc-Carabin
CsA
kDa
H3K4Me1 17
C-Myc 50
H3 17
D
-PE
+PE
siCT
siMLL3
10 µm
5E-4
4E-4
0.76
Cell Surface (% of Si-CT)
-PE +PE -PE +PE
siCT siMLL3
E
acta1
0.045
0.027
0.749
acta1 mRNA (R.Q.)
-PE +PE -PE +PE
siCT siMLL3
F
nppb
1E-4
0.041
0.348
nppb mRNA (R.Q.)
-PE +PE -PE +PE
siCT siMLL3

**Figure 2. MLL3 promotes cardiac hypertrophy.**

**A,** Quantification of H3K4Me1 level in NRVMs treated with PE (10 µM) for the indicated times (n=7). Representative immunoblots are shown. **B-C,** Immunoblot analysis showing the effect of siRNA against Carabin (SiCarabin) or MLL3 (siMLL3), CsA (1 µM, 1 h), Carabin overexpression or pcDNA3 control vector on H3K4Me1 level in NRVMs treated or not with PE (10 µM, 3 h). (B, n=9 ; C n=8). Values are normalised to the siCT, -PE condition. **D,** *top,* Immunofluorescence staining of sarcomeric α-actinin (red) in siCT or siMLL3-transfected NRVM treated (+PE) or not (-PE) with PE (10 µM, 24 h). DNA is stained with DAPI (blue), Scale Bar: 10 µm. *bottom*, quantification of cardiomyocyte area. >250 NRVM per condition from 4 independent cell culture preparations were analysed. Values are normalised to the siCT, -PE condition. Each point represents an individual cell. Differences between groups were analyzed by a nested one-way ANOVA. **E-F,** Relative expression of cardiomyocyte hypertrophy gene markers (*acta1, nppb*) in siCT or siMLL3-transfected NRVMs treated (+PE) or not (-PE) with PE (10 µM, 24 h) (n= 6). Results are expressed as mean ± SEM. Differences between groups were analyzed by a Friedman test with a two-stage linear step-up procedure of Benjamini, Krieger and Yekutieli (A) and a Krukal-Wallis test with a two-stage linear step-up procedure of Benjamini, Krieger and Yekutieli (B, C, E, F). Black lines indicate compared groups with the corresponding p-value. Differences were considered significant when $P<0.05$.

Figure 3

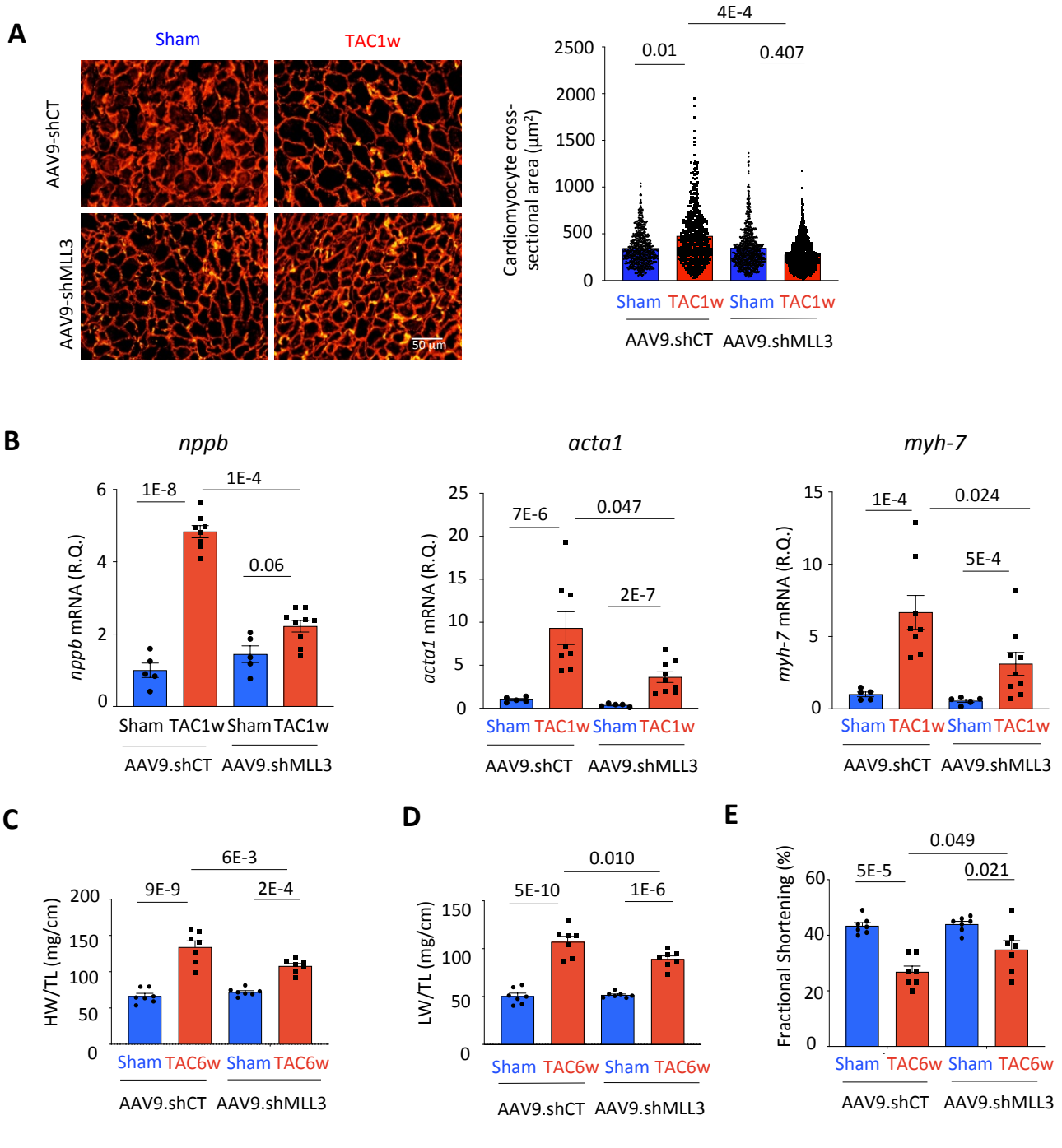
A
Sham
TAC1w
AAV9-shCT
AAV9-shMLL3
50 µm
4E-4
0.01
0.407
Cardiomyocyte cross-sectional area (µm²)
2500
2000
1500
1000
500
0
Sham TAC1w Sham TAC1w
AAV9.shCT AAV9.shMLL3
B
nppb
1E-8
1E-4
0.06
nppb mRNA (R.Q.)
6
4
2
0
Sham TAC1w Sham TAC1w
AAV9.shCT AAV9.shMLL3
acta1
7E-6
0.047
2E-7
acta1 mRNA (R.Q.)
25
20
15
10
5
0
Sham TAC1w Sham TAC1w
AAV9.shCT AAV9.shMLL3
myh-7
1E-4
0.024
5E-4
myh-7 mRNA (R.Q.)
15
10
5
0
Sham TAC1w Sham TAC1w
AAV9.shCT AAV9.shMLL3
C
6E-3
9E-9
2E-4
HW/TL (mg/cm)
200
150
100
50
0
Sham TAC6w Sham TAC6w
AAV9.shCT AAV9.shMLL3
D
0.010
5E-10
1E-6
LW/TL (mg/cm)
150
100
50
0
Sham TAC6w Sham TAC6w
AAV9.shCT AAV9.shMLL3
E
0.049
5E-5
0.021
Fractional Shortening (%)
60
40
20
0
Sham TAC6w Sham TAC6w
AAV9.shCT AAV9.shMLL3

**Figure 3. MLL3 binds to the transcriptional start site (TSS) of genes associated to cardiomyopathy.**

**A,** Representative images of vinculin stained heart sections (Scale bar: 50 μm) of AAV9-shCT or AAV9-shMLL3 treated mice subjected or not to 1 week TAC. The bar graphs on the right show the quantification of cardiomyocyte cross-sectional areas. >80 cardiomyocytes per mouse were analysed (n=5 mice per Sham group and n=6 mice per TAC group). Each point represents an individual cell. Differences between groups were analyzed by a nested one-way ANOVA. **B,** Relative expression of cardiac hypertrophy gene markers (*nppb*, *acta1, myh-7*) in control AAV9-shCT or AAV9-shRNA MLL3 treated mice subjected or not to TAC surgery for 1 week (n=5 per Sham group ; n= 8 and 9 mice in TAC AAV9.shCT and AAV9.shMLL3 respectively). Results are expressed relative to AAV9.shCT Sham mice. **C-E**, Heart weight (HW) normalized to tibia length (TL) (C), lung weight (LW) normalized to tibia length (TL) (D), Fractional Shortening (E) of control AAV9-shCT or AAV9-shRNA MLL3 treated mice subjected or not to TAC surgery for 6 weeks (n=7 mice/group).
Results are expressed as mean ± SEM. Statistics analyses were performed on log-transformed values (B). Differences between groups were analyzed by a one-way ANOVA (B-E). Black lines indicate compared groups with the corresponding p-value. Differences were considered significant when $P<0.05$.

Figure 4

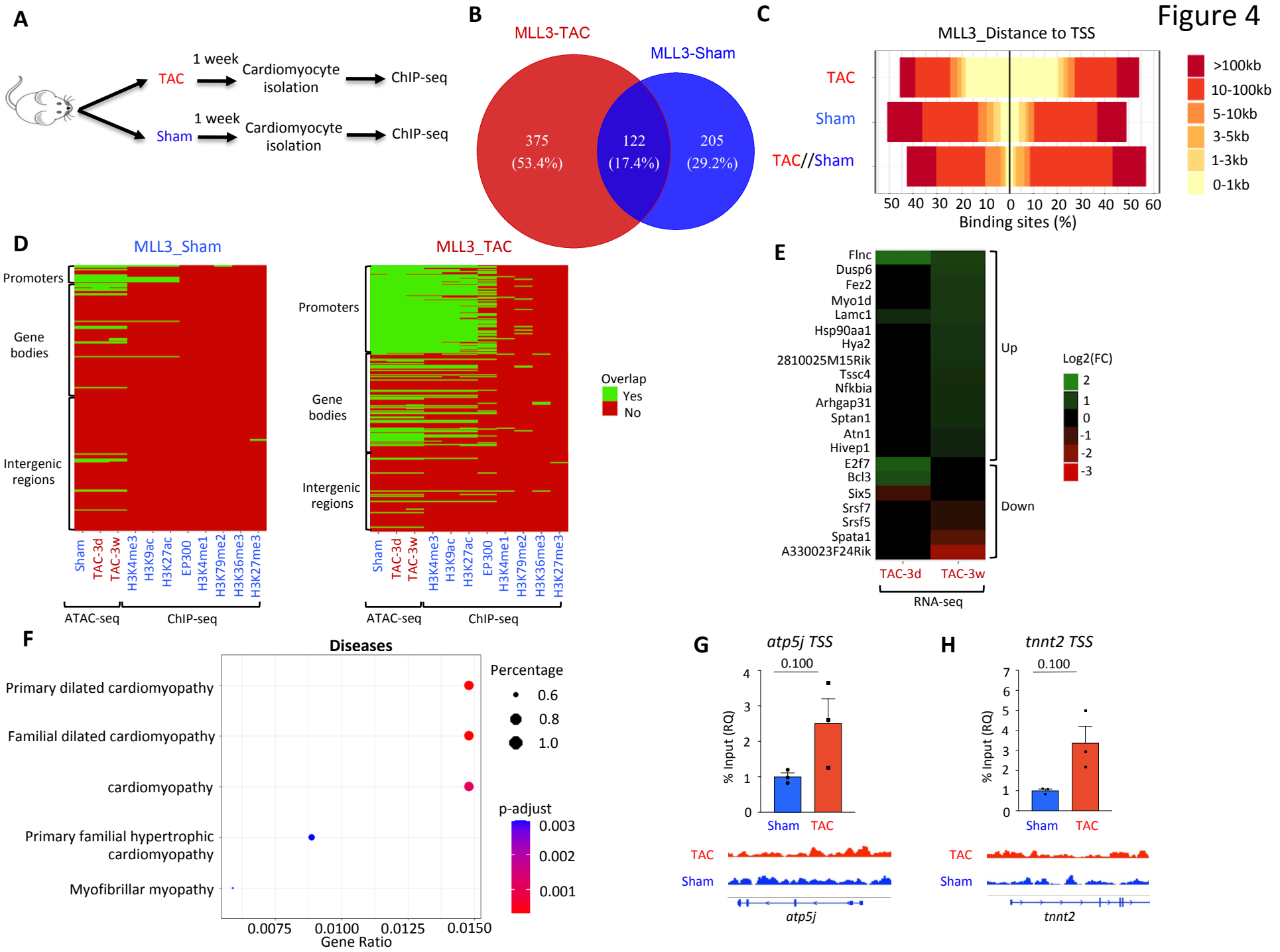
A
TAC
1 week
Cardiomyocyte isolation
ChIP-seq
Sham
1 week
Cardiomyocyte isolation
ChIP-seq
B
MLL3-TAC
MLL3-Sham
375 (53.4%)
122 (17.4%)
205 (29.2%)
C
MLL3_Distance to TSS
TAC
Sham
TAC//Sham
>100kb
10-100kb
5-10kb
3-5kb
1-3kb
0-1kb
50 40 30 20 10 0 10 20 30 40 50 60
Binding sites (%)
D
MLL3_Sham
MLL3_TAC
Promoters
Gene bodies
Intergenic regions
Sham
TAC-3d
TAC-3w
H3K4me3
H3K9ac
H3K27ac
EP300
H3K4me1
H3K79me2
H3K36me3
H3K27me3
ATAC-seq
ChIP-seq
Overlap
Yes
No
E
Flnc
Dusp6
Fez2
Myo1d
Lamc1
Hsp90aa1
Hya2
2810025M15Rik
Tssc4
Nfkbia
Arhgap31
Sptan1
Atn1
Hivep1
E2f7
Bcl3
Six5
Srsf7
Srsf5
Spata1
A330023F24Rik
Up
Down
Log2(FC)
2
1
0
-1
-2
-3
TAC-3d
TAC-3w
RNA-seq
F
Diseases
Primary dilated cardiomyopathy
Familial dilated cardiomyopathy
cardiomyopathy
Primary familial hypertrophic cardiomyopathy
Myofibrillar myopathy
0.0075 0.0100 0.0125 0.0150
Gene Ratio
Percentage
0.6
0.8
1.0
p-adjust
0.003
0.002
0.001
G
atp5j TSS
0.100
% Input (RQ)
Sham
TAC
TAC
Sham
atp5j
H
tnnt2 TSS
0.100
% Input (RQ)
Sham
TAC
TAC
Sham
tnnt2

**Figure 4. MLL3 binds to the transcriptional start site (TSS) of genes associated to cardiomyopathy.**

**A,** Schematic of the ChIP-seq experimental workflow. **B**, Overlap of MLL3 binding in Sham and TAC conditions revealed by ChIP-seq. The numbers and percentages of peaks are shown on the diagram. **C**, Distribution of MLL3 Sham-specific, TAC-specific and Sham and TAC- cobound loci relative to TSS. **D**, DNA accessibility and histone post-translational profile of TAC- and Sham-specific MLL3 bound genomic regions. **E**, Heatmap representing the expression levels of the TAC-specific MLL3-targeted genes differentially regulated in 3 days- and 3 weeks-post TAC mouse hearts. Green and red coloring represent respectively increase and decrease expression level. **F**, Gene ontology analysis showing the diseases associated with the genes located closest to the TAC-specific MLL3 binding sites. **G-H**, MLL3 ChIP-qPCR on *atp5j* and *tnnt2* Transcription Start Site (TSS) on isolated cardiomyocytes from sham or TAC mice. Data were normalized over Input. Data are represented as mean ± SEM of 3 independent experiments. The distribution of reads obtained by ChIP-seq is shown below the ChIP-qPCR quantification graph. Results are expressed as mean ± SEM and normalised to Sham condition. Differences between groups were analyzed by a Mann-Whitney U test on log-transformed data (G-H). Black lines indicate compared groups with the corresponding p-value. Differences were considered significant when $P<0.05$.

Figure 5

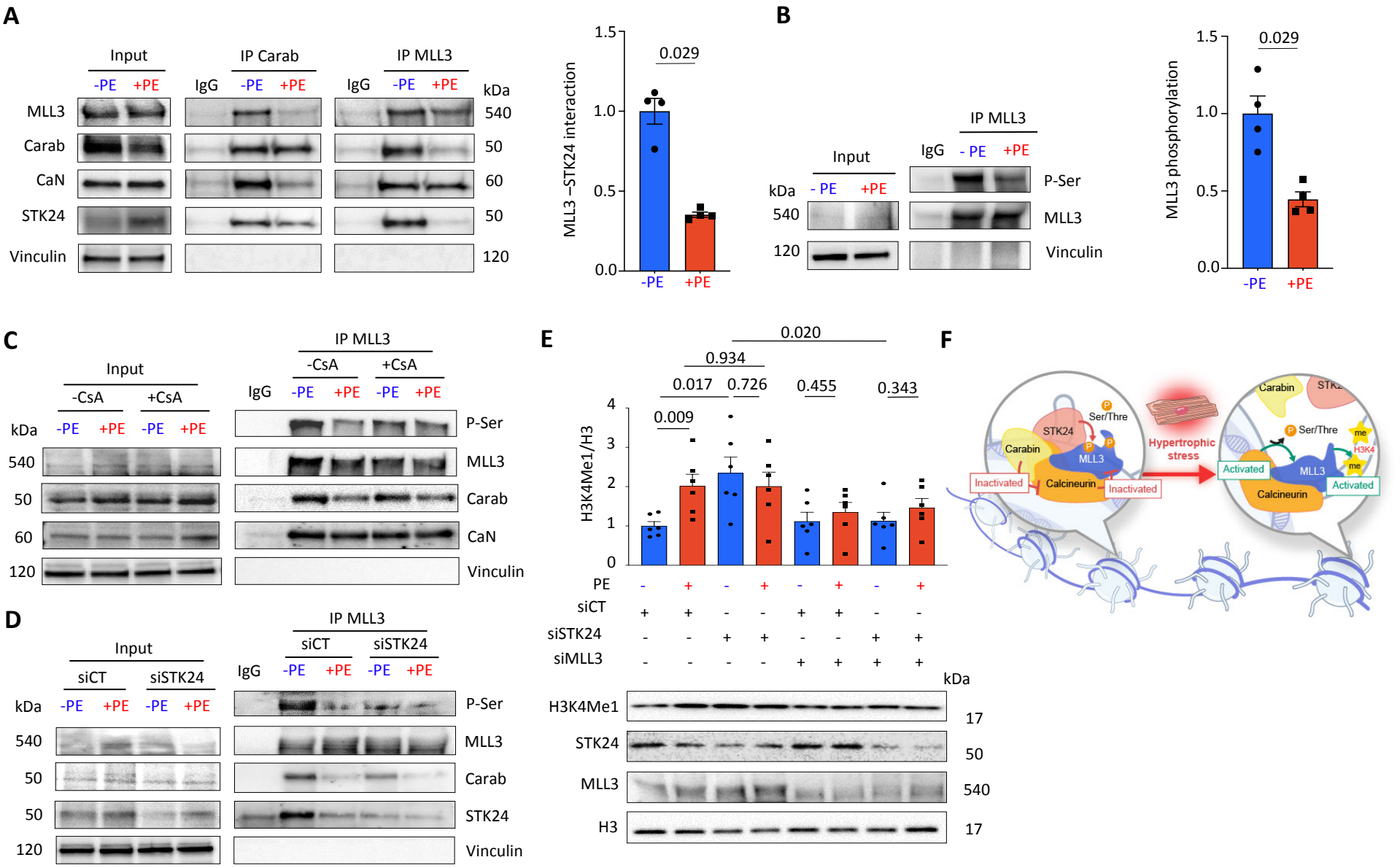
A
Input
IP Carab
IP MLL3
-PE +PE
IgG -PE +PE
IgG -PE +PE
kDa
MLL3
Carab
CaN
STK24
Vinculin
540
50
60
50
120
B
MLL3 –STK24 interaction
0.029
1.5
1.0
0.5
0.0
-PE +PE
Input
IP MLL3
IgG - PE +PE
kDa
540
120
P-Ser
MLL3
Vinculin
MLL3 phosphorylation
0.029
C
Input
-CsA +CsA
IP MLL3
-CsA +CsA
IgG -PE +PE -PE +PE
kDa -PE +PE -PE +PE
540
50
60
120
P-Ser
MLL3
Carab
CaN
Vinculin
D
Input
siCT siSTK24
IP MLL3
siCT siSTK24
IgG -PE +PE -PE +PE
kDa -PE +PE -PE +PE
540
50
50
120
P-Ser
MLL3
Carab
STK24
Vinculin
E
0.020
0.934
0.017 0.726
0.455
0.343
0.009
H3K4Me1/H3
4
3
2
1
0
PE - + - + - + - +
siCT + + - - + + - -
siSTK24 - - + + - - + +
siMLL3 - - - - + + + +
kDa
H3K4Me1
STK24
MLL3
H3
17
50
540
17
F
Carabin
STK24
Ser/Thre
MLL3
Calcineurin
Inactivated
Inactivated
Hypertrophic stress
Activated
Activated
me
H3K4

**Figure 5. Calcineurin and STK24 display opposite action on MLL3 HMT activity.**

**A,** *Left*- Representative immunoblot of Immunoprecipitation (IP) experiments showing the interaction of Carabin (Carab) or MLL3 with MLL3, Carabin (Carab), calcineurin (CaN), and STK24 in NVRM stimulated or not with PE (10 µM, 30 min) (n=4). *Right*- Histogram showing the ratio of immunoprecipitated STK24 to immunoprecipitated MLL3 in NRVMs treated or not with PE (10 µM, 30 min). **B**, Representative immunoblot and quantification histogram of MLL3 immunoprecipitation experiments showing MLL3 phosphorylation state in NRVMs treated or not with PE (10 µM, 30 min) (n=4). **C,** Immunoprecipitation experiments showing that cyclosporin A (CsA, 1 µM, 1 h) prevented MLL3 phosphorylation at serine residue in NRVMs treated with PE (10 µM, 30 min) (n=3). **D**, Immunoprecipitation analysis showing the effect of siRNA against STK24 (siSTK24) or siRNA control (siCT) on MLL3 phosphorylation in NRVMs stimulated or not with PE (10 µM, 30 min) (n=3). **E**, Effect of siMLL3 or siSTK24 on H3K4Me1 levels in NRVMs in the absence or presence of PE (10 µM, 3h). The bar graphs represent the quantification of H3K4Me1 (n=6). Input, cell lysates. Results are expressed as mean ± SEM and normalised to –PE (A, B) and siCT (E). Differences between groups were analyzed by a Mann-Whitney U test (A, B), a Krukal-Wallis test with two-stage linear step-up procedure of Benjamini, Krieger and Yekutieli (E). Black lines indicate compared groups with the corresponding p-value. Differences were considered significant when $P<0.05$. **F**, Schematic representation of the molecular mechanisms regulating MLL3 histone methyl transferase (HMT) activity. In basal condition, MLL3 is bound to a molecular complex containing STK24, Carabin and calcineurin. Within this complex, Carabin exerts a negative action on calcineurin Ser/Thr phosphatase activity and STK24 maintains MLL3 phosphorylated at Ser residue. Under hypertrophic stress, Carabin and STK24 are released from the complex leading to calcineurin activation and the subsequent dephosphorylation of MLL3 promotes MLL3 HMT activity.

Figure 6

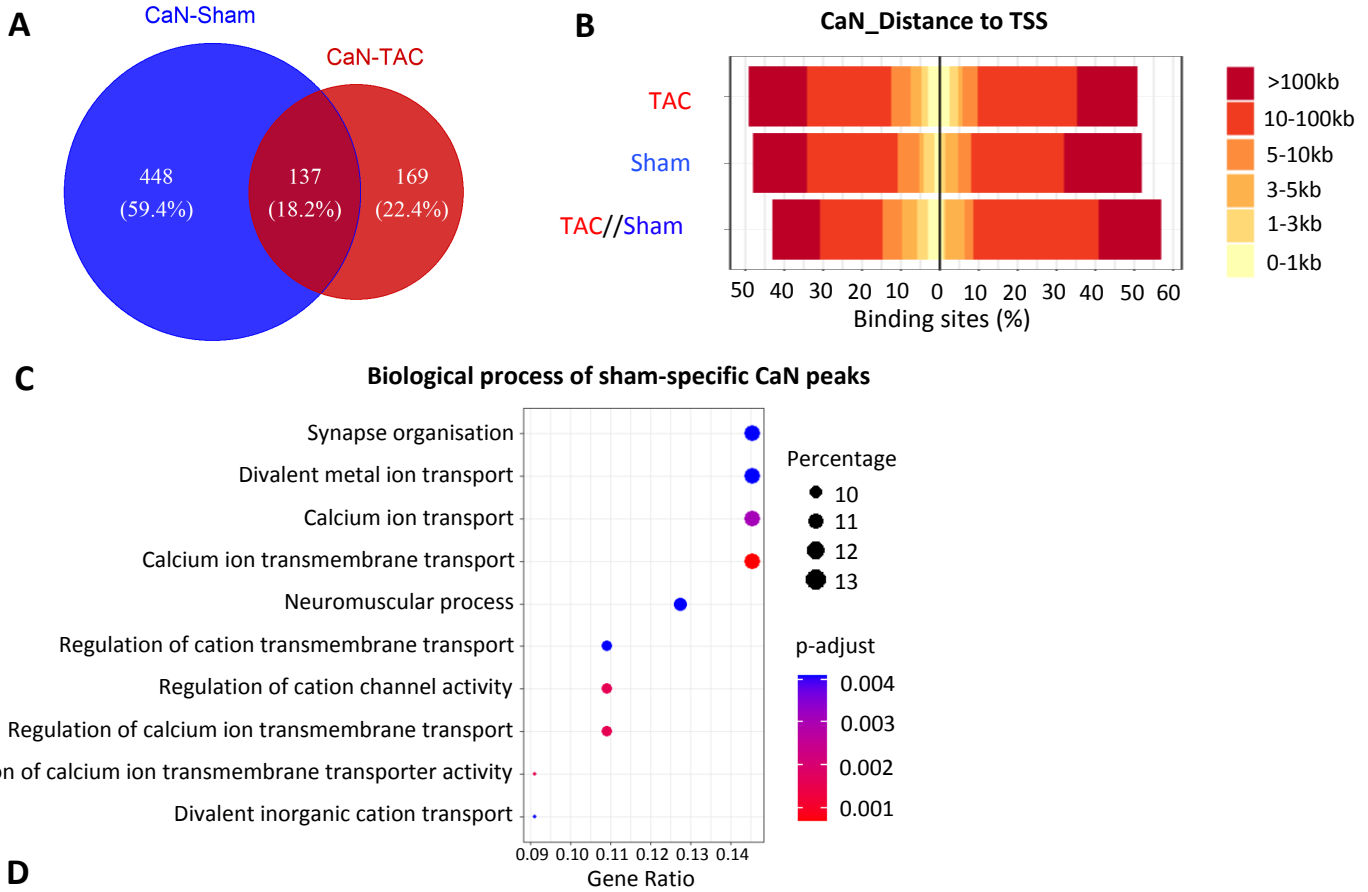
A
CaN-Sham
CaN-TAC
448
(59.4%)
137
(18.2%)
169
(22.4%)
B
CaN_Distance to TSS
TAC
Sham
TAC//Sham
50 40 30 20 10 0 10 20 30 40 50 60
Binding sites (%)
>100kb
10-100kb
5-10kb
3-5kb
1-3kb
0-1kb
C
Biological process of sham-specific CaN peaks
Synapse organisation
Divalent metal ion transport
Calcium ion transport
Calcium ion transmembrane transport
Neuromuscular process
Regulation of cation transmembrane transport
Regulation of cation channel activity
Regulation of calcium ion transmembrane transport
Regulation of calcium ion transmembrane transporter activity
Divalent inorganic cation transport
0.09 0.10 0.11 0.12 0.13 0.14
Gene Ratio
Percentage
10
11
12
13
p-adjust
0.004
0.003
0.002
0.001
D
Motif analysis : CaN binding sites in sham
ETS2 (p=4.12e-04)
IRF8 (p=1.48e-03)
ETV2 (p=2.71e-03)
BRAC (p=6.43e-04)
HAX1 (p=2.18e-03)
PBX2 (p=2.26e-03)
ERG2 (p=1.99e-03)
Motif analysis : CaN binding sites in TAC
NFatc4 (p=2.26e-03)
ELF1 (p=5.63e-04)
GABPA (p=1.77e-03)
LYL1 (p=1.92e-03)

**Figure 6. Calcineurin is recruited on chromatin at intergenic regions**

**A,** Overlap of calcineurin binding in Sham and TAC conditions revealed by ChIP-seq analysis. The number and percentage of peaks within each category are shown on the diagram. **B,** Distribution of calcineurin Sham-specific, TAC-specific and Sham and TAC- cobound loci relative to TSS. **C**, Gene Ontology analysis showing the biological processes associated with the genes located closest to the sham-specific calcineurin binding sites. **D**, *De novo* MEME motif discovery analysis of calcineurin binding sites in Sham and TAC conditions. Motif analysis revealed enrichment in the indicated transcription factors.

Figure 7

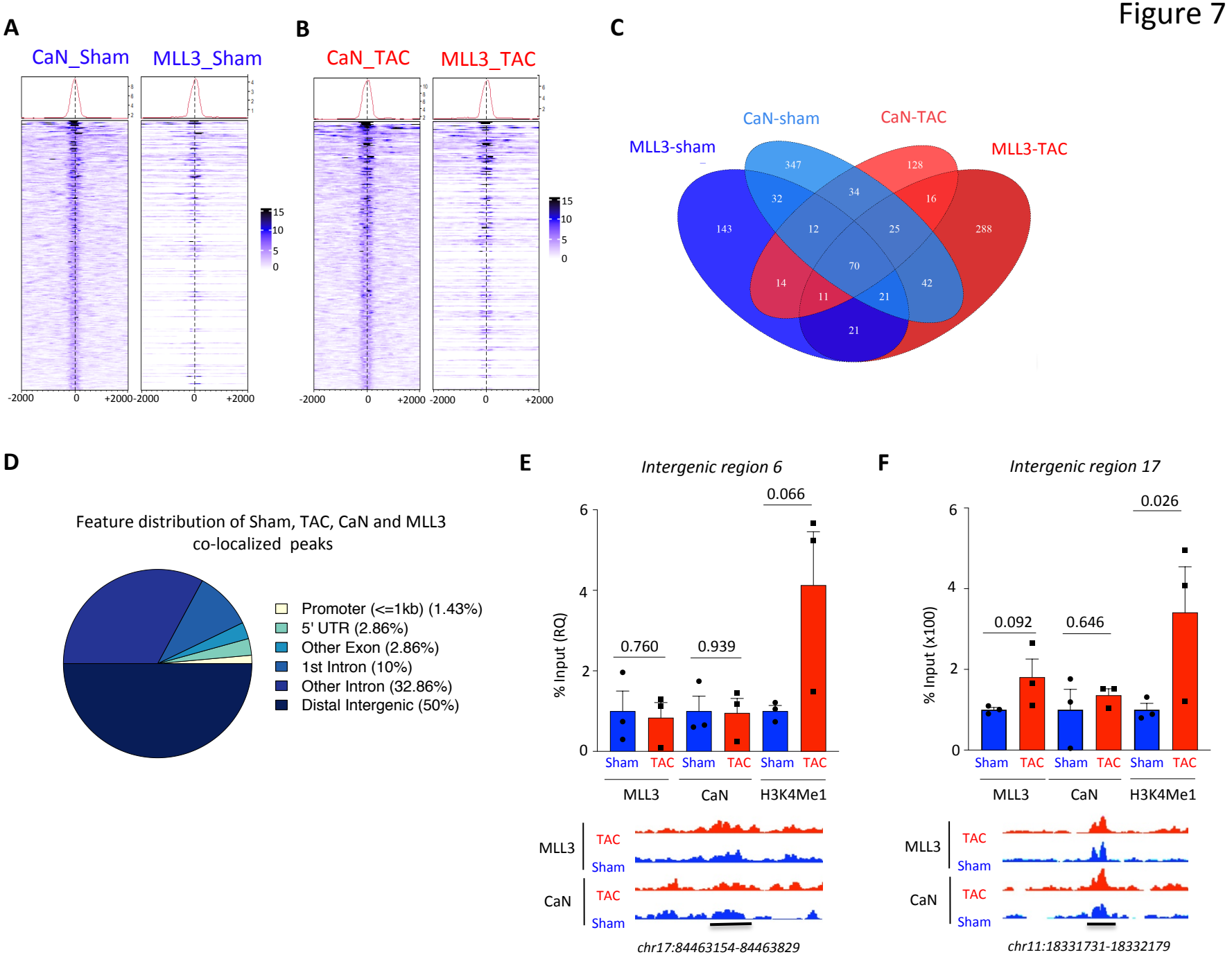
A
CaN_Sham
MLL3_Sham
B
CaN_TAC
MLL3_TAC
C
CaN-sham
CaN-TAC
MLL3-sham
MLL3-TAC
D
Feature distribution of Sham, TAC, CaN and MLL3 co-localized peaks
Promoter (<=1kb) (1.43%)
5' UTR (2.86%)
Other Exon (2.86%)
1st Intron (10%)
Other Intron (32.86%)
Distal Intergenic (50%)
E
Intergenic region 6
% Input (RQ)
0.760
0.939
0.066
Sham
TAC
MLL3
CaN
H3K4Me1
chr17:84463154-84463829
F
Intergenic region 17
% Input (x100)
0.092
0.646
0.026
chr11:18331731-18332179

**Figure 7. Calcineurin colocalises with MLL3 on chomatin.**

**A**-**B**. Heatmap of Calcineurin binding regions showing binding signal intensity for MLL3 in Sham (A) and TAC (B) conditions. Binding is ranked from the strongest to the weakest binding sites. **C**, Venn diagram showing the overlap of calcineurin and MLL3 binding in sham and TAC conditions revealed by ChIP-seq. The numbers of peaks within each category are shown on the diagram. **D,** Genomic distribution of MLL3 and calcineurin 70 co-bound peaks in sham and TAC conditions. Genomic regions are color coded according to the labels on the right. **E-F**, MLL3, calcineurin and H3K4me1 ChIP-qPCR quantification of two intergenic regions bound by the MLL3-calcineurin complex in adult cardiomyocytes isolated from Sham or TAC mice (n=3). Data were normalized over Input. Results are expressed relative to sham condition and as mean ± SEM (E, F). Differences between groups were analyzed by Krukal-Wallis test with two-stage linear step-up procedure of Benjamini, Krieger and Yekutieli. The distribution of reads obtained by ChIP-seq is shown below the ChIP-qPCR quantification graph. Black lines indicate compared groups with the corresponding p-value.

# TABLES

Table 1

| | Sham-AAV9.shCt (n=13) | TAC-AAV9.shCt (n=18) | Sham-AAV9.shMLL3 (n=12) | TAC-AAV9.shMLL3 (n=19) |
|---|---|---|---|---|
| **LVIDd, mm** | 3.49 ± 0.07 | 3.40 ± 0.04 | 3.34 ± 0.05 | 3.26 ± 0.05 |
| **LVIDs, mm** | 2.1 ± 0.06 | 2.0 ± 0.07 | 1.95 ± 0.06 | 1.96 ± 0.06 |
| **FS, %** | 39.69 ± 0.81 | 39.74 ± 1.79 | 41.58 ± 1.42 | 39.21 ± 1.35 |
| **Heart rate, $min^{-1}$** | 587.00 ± 21.00 | 595.10 ± 12.16 | 586.00 ± 9.55 | 578.10 ± 15.06 |
| **Pseudomass** | 87.07 ± 3.53 | 115.26 ± 4.07 6E-6 | 77.25 ± 2.00 | 95.89 ± 3.53 *5E-3* **7E-4** |
| **LVAWd, mm** | 0.83 ± 0.02 | 1.04 ± 0.02 6E-8 | 0.79 ± 0.02 | 0.93 ± 0.03 *1E-3* **1E--3** |
| **LVPWd, mm** | 0.74 ± 0.02 | 0.90 ± 0.03 5E-4 | 0.71 ± 0.01 | 0.87 ± 0.03 *0.001* |

**Table 1. Echocardiographic Analysis of Sham and 1 week post TAC mice injected with AAV9.shCT and AAV9.shMLL3**

LVIDd indicates left ventricular end-diastolic internal diameter; LVIDs, left ventricular end-systolic internal diameter; FS, fractional shortening; LVAWd, left ventricular anterior wall in diastole; LVPWd, left ventricular posterior wall in diastole; TAC, transverse aortic constriction. Pseudomass was derived from echocardiography analyses, LV mass was calculated from short axis M-mode view according to the formula, which gives estimated heart weight values in mg: $(LVID,d + LVAW,d + LVPW,d)^{\wedge 3} – LVID,d^{\wedge 3}$.

Results are expressed as mean ± SEM. Statistical significance was determined by one-way ANOVA tests with Tukey's multiple comparisons test. p-values are indicated using superscripts for TAC-AAV9.shCt vs Sham-AAV9.shCt, superscripts in italics for TAC-AAV9.shMLL3 vs Sham-AAV9.shMLL3 and bold superscripts for TAC-AAV9.shCt vs TAC-AAV9.shMLL3 comparisons. Differences were considered significant at $p<0.05$.

Table 2

| | Sham-AAV9.shCt (n=7) | TAC-AAV9.shCt (n=7) | Sham-AAV9.shMLL3 (n=7) | TAC-AAV9.shMLL3 (n=7) |
|---|---|---|---|---|
| **LVIDd, mm** | 3.47 ± 0.09 | 3.35 ± 0.08 | 3.38 ± 0.06 | 3.11 ± 0.06 |
| **LVIDs, mm** | 2.07 ± 0.09 | 2.09 ± 0.15 | 2.01 ± 0.08 | 1.90 ± 0.05 |
| **FS, %** | 43.43 ± 1.13 | 26.86 ± 2.06 5E-5 | 44.00 ± 1.02 | 34.86 ± 3.2 *0.021;* **0.049** |
| **Heart rate, $min^{-1}$** | 569.43 ± 24.28 | 550.29 ± 20.76 | 541.57 ± 17.36 | 530.29 ± 26.43 |
| **Pseudomass** | 86.43 ± 5.28 | 125.14 ± 7.90 6E-4 | 77.86 ± 1.84 | 91.00 ± 6.99 **0.002** |
| **LVAWd, mm** | 0.82 ± 0.04 | 1.04 ± 0.06 0.007 | 0.78 ± 0.03 | 0.94 ± 0.04 |
| **LVPWd, mm** | 0.76 ± 0.04 | 1.00 ± 0.05 0.002 | 0.72 ± 0.03 | 0.87 ± 0.05 |

**Table 2. Echocardiographic Analysis of Sham and 6 weeks post-TAC mice injected with AAV9.shCT and AAV9.shMLL3**

LVIDd indicates left ventricular end-diastolic internal diameter; LVIDs, left ventricular end-systolic internal diameter; FS, fractional shortening; LVAWd, left ventricular anterior wall in diastole; LVPWd, left ventricular posterior wall in diastole; TAC, transverse aortic constriction. Pseudomass was derived from echocardiography analyses, LV mass was calculated from short axis M-mode view according to the formula, which gives estimated heart weight values in mg: $(LVID,d + LVAW,d + LVPW,d)^{\wedge 3} – LVID,d^{\wedge 3}$.

Results are expressed as mean ± SEM. Statistical significance was determined by one-way ANOVA tests with Tukey's multiple comparisons test.

p-values are indicated using superscripts for TAC-AAV9.shCt vs Sham-AAV9.shCt, superscripts in italics for TAC-AAV9.shMLL3 vs Sham-AAV9.shMLL3 and bold superscripts for TAC-AAV9.shCt vs TAC-AAV9.shMLL3 comparisons. Differences were considered significant at $p<0.05$.